Teaching Case

Anaplastic Ependymoma and Posterior Fossa Grouping in a Patient With H3K27ME3 Loss of Expression but Chromosomal Imbalance

David M. Routman MD [a], Aditya Raghunathan MD, MPH [b],
Caterina Giannini MD, PhD [b], Anita Mahajan MD [a],
Chris Beltran PhD [a], Mahmoud G. Nagib MD [c],
Amulya A. Nageswara Rao MBBS [d], Mary M. Skrypek MD [e],
Nadia N.I. Laack MD, MS [a],*

[a]Department of Radiation Oncology, Mayo Clinic, Rochester, Minnesota; [b]Laboratory Medicine and Pathology, Mayo Clinic, Rochester, Minnesota; [c]Department of Neurosurgery, University of Minnesota, Minneapolis, Minnesota; [d]Division of Pediatric Hematology Oncology, Mayo Clinic, Rochester, Minnesota; and [e]Department of Hematology Oncology, Children's Minnesota, Minneapolis, Minnesota

Introduction

Ependymoma represents the third most common childhood malignancy of the brain, accounting for approximately 10% of all pediatric brain malignancies.[1] The most common site of presentation is the posterior fossa.[1] Standard therapy involves maximal safe resection, followed by radiation therapy (RT).[2] The benefit of chemotherapy (CHT) has not been demonstrated and remains under investigation.[3,4] Molecular analysis has identified 2 groups within ependymomas of the posterior fossa (PF-EPN) with distinct prognoses and characteristics (Table 1): group A (PF-EPN-A) and group B (PF-EPN-B).[5,6] Grouping is prognostic, but World Health Organization (WHO) II versus III grade designation is not reliably prognostic.[7-9] Therefore, current consensus guidelines recommend that treatment decisions not be based solely on histopathologic characteristics but incorporate molecular analysis.[10]

To date, no prospective trials have been completed on the basis of PF-EPN grouping to guide management. Standard of care remains the same for both groups: maximal safe resection, followed by RT. Both groups have been shown to benefit from gross total resection on retrospective analysis with the more favorable PF-EPN-B patients still having significantly worse outcomes with subtotal resection, as demonstrated in a large analysis by Ramaswamy et al.[11] This analysis also evaluated adjuvant RT by group, but the conclusions were limited by comparisons across groups with different treatment strategies and by patient numbers, and no benefit of adjuvant RT was demonstrated for PF-EPN-B patients.[11]

H3K27me3 represents trimethylation of lysine on the histone complex and has been shown to be a high-quality and cost-effective test that discriminates PF-EPN-A from PF-EPN-B, with loss of expression of this marker originally shown to overlap precisely with A grouping.[12] A more recent analysis of 112 pediatric ependymomas with known methylation-based PF-EPN subgrouping revealed a sensitivity of 99% and specificity of 100% for H3K27me3 loss of expression in discerning the

* Corresponding author. Radiation Oncology, Mayo Clinic, 200 First Street SW, Rochester, MN 55905.

E-mail address: Laack.nadia@mayo.edu (N.N.I. Laack).

Table 1   Characteristics of ependymoma of the posterior fossa group A compared with group B

Group A	Group B
▪ Predominantly infants and young children	▪ Predominantly children >5 y old
▪ More common in male than female children	▪ More common in female than male children
▪ Often more lateralized	▪ Centrally located
▪ Hypothesized to be less amenable to gross total resection	▪ Hypothesized to be more amenable to gross total resection
▪ Carries a worse prognosis	▪ Better prognosis
▪ Chromosomal balance	▪ Chromosomal instability

subgroups, with the loss of H3K27me3 expression associated with significantly worse progression-free and overall survival.[13] One of 40 cases with PF-EPN-B tumors (2.5%) demonstrated a methylation array profile that corresponded to PF-EPN-B but had an unexpected loss of expression.[13]

Herein, we report on an additional case of an 8-year-old patient with a posterior fossa anaplastic ependymoma (WHO grade III) that harbors chromosomal instability corresponding to the PF-EPN-B subgroup based on chromosomal microarray analysis but has discordant loss of H3K27me3 expression by immunohistochemistry. In this context, we consider the patient's presentation, treatment, course, and implications of grouping for future research and clinical trials.

Case

Initial presentation and resection

An 8-year-old male patient had progressive headaches over 1 year, eventually associated with nausea and vomiting. The headaches worsened in severity, and he was seen at the emergency department where a computed tomography (CT) head scan demonstrated a large partially cystic mass of the posterior fossa with associated obstructive hydrocephalus. The patient underwent an endoscopic third ventriculostomy with an extra ventricular drain placement. A magnetic resonance imaging (MRI) scan revealed a 7.8 × 7.0 × 8.0 cm mass centered in the right foramen of Luschka versus the right middle cerebellar peduncle with extension superiorly into the supratentorial compartment (Figs 1A and B). The patient underwent an extensive resection of both the infratentorial and supratentorial components, using intracranial neuronavigation, with a cerebellopontine angle and posterior temporal craniotomy. The surgery involved microdissection and exposure of the basilar artery and facial and trigeminal nerves and an intra-operative MRI. The resection was ultimately classified as a subtotal resection given concern for residual disease, including in the fourth ventricle (Fig 1C). MRI of the spine and postoperative lumbar puncture were negative.

Pathology

The hematoxylin and eosin—stained histologic sections revealed a hypercellular neoplasm with widespread perivascular pseudo-rosette formation, composed of cells with fibrillary cytoplasmic processes and oval-to-elongated nuclei with stippled chromatin (Fig 2A). Immunohistochemical staining was performed on the formalin-fixed, paraffin-embedded sections, and the neoplastic cells tested positive for glial fibrillary acidic protein (polyclonal; Dako), supporting glial differentiation and highlighting perivascular cytoplasmic processes. No axons were identified within the tumor by Neurofilament (clone 2F11; Dako), consistent with a solid growth pattern. In few foci, the tumor cells were found to harbor paranuclear, dot-like expression of the epithelial membrane antigen (clone E29; Dako). This immunostaining pattern was consistent with an ependymoma. Many regions of the ependymoma were hypercellular (exhibiting cells with increased nuclear-to-cytoplasmic ratios and nuclear crowding; Fig 2B) and harbored brisk mitotic activity (>6 mitoses per 10 consecutive 400× magnification fields). Foci of tumor necrosis were also identified, supporting a diagnosis of anaplastic ependymoma (WHO grade III).

The ependymoma cells showed widespread loss of expression of H3K27me3 (clone C36B11; cell signaling; Fig 2C). Chromosomal microarray analysis was performed using molecular inversion probes on a whole genome array (Affymetrix Oncoscan platform) and demonstrated an abnormal molecular karyotype with chromosomal instability, characterized by loss of whole chromosomes 1 (including *AJAP1*), 3, 6, 9 (including *CDKN2A/B*), 10 (including *PTEN*), 11, 12, 14, 15, 16, 18, and X in approximately 50% of cells and loss of chromosome 22 (including *NF2*) in 100% of cells (Fig 3). Of note, no chromothriptic events on chromosome 11 or abnormalities suggestive of a *RELA* or *YAP1* rearrangement were observed.
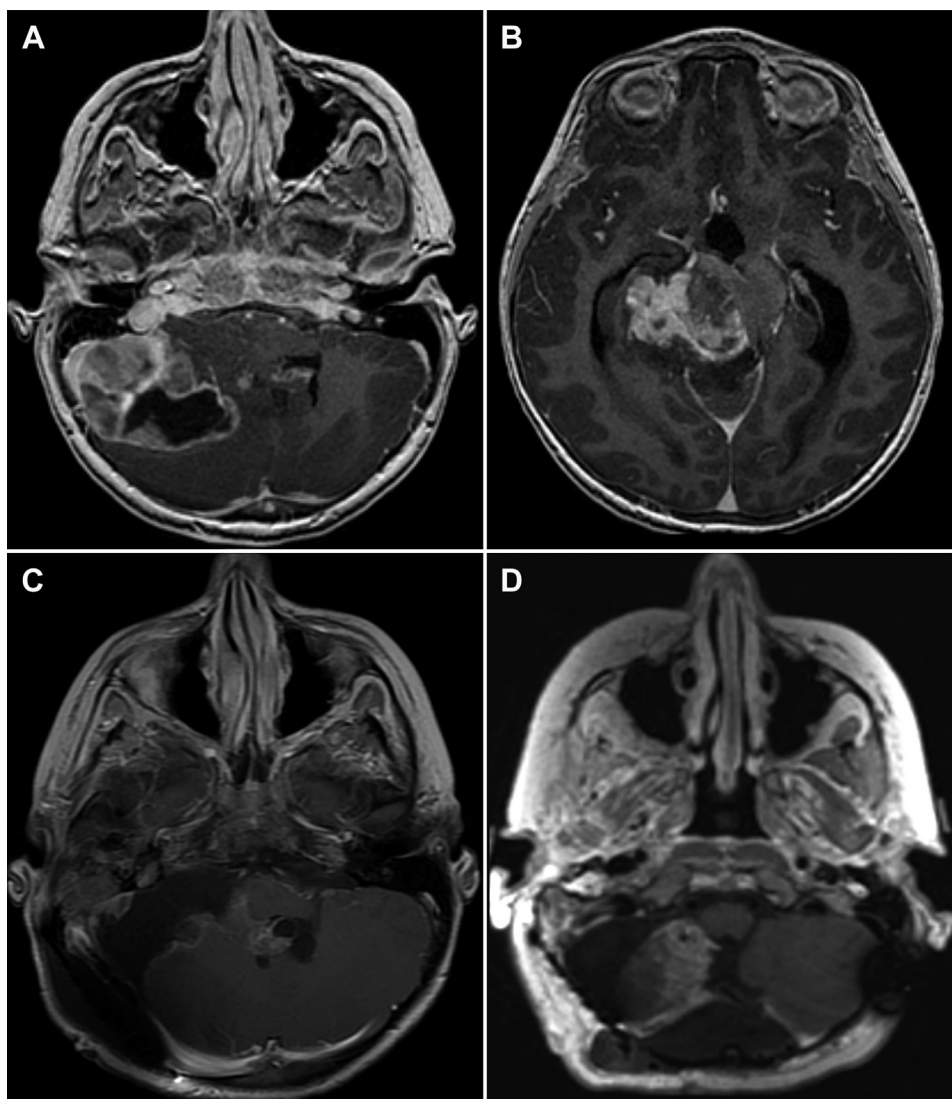
Figure 1 Pre- and postoperative imaging. (A) Axial T1 3-dimensional post-gad magnetic resonance imaging (MRI) at presentation, showing lateralized tumor with ventricular and brainstem compression and (B) supratentorial component. (C) Axial Se T1 post-gad MRI, demonstrating resection with residual fourth ventricular disease, and (D) Axial T1 cub reformat post-gad MRI after receipt of chemotherapy and second-look surgery

Postoperative course, chemotherapy, and subsequent treatment strategy

The patient's postoperative course was complicated by numbness and weakness of the right side of his face as well as dysphagia and aspiration, infection, and changes in speech, with initial reliance on a percutaneous endoscopic gastrostomy tube. He gradually improved in all domains, tolerating a nectar thick liquid diet and solid foods, with improvement in speech.

The patient was enrolled on ACNS 0831 and, given his residual disease, received induction CHT, including vincristine, carboplatin, and cyclophosphamide for cycle A and vincristine, carboplatin, and etoposide for cycle B. Baseline audiology examination before CHT revealed no appreciable hearing on the right side. The patient underwent reimaging per protocol, and residual enhancement previously noted was unchanged. After consultation with radiation oncology and neurosurgery and a multidisciplinary discussion, the patient underwent a re-resection of the fourth ventricular disease with a posterior approach via the vermis (Fig 1D). The patient recovered well from this second operation with no new deficits. Pathology test results were positive, revealing ependymal cells with treatment effect.

Radiation therapy

The patient was seen for consideration of adjuvant RT, and treatment was recommended per protocol. A CT simulation and MRI in treatment position were performed. Treatment was delivered using pencil beam scanning proton therapy and multifield optimization to a
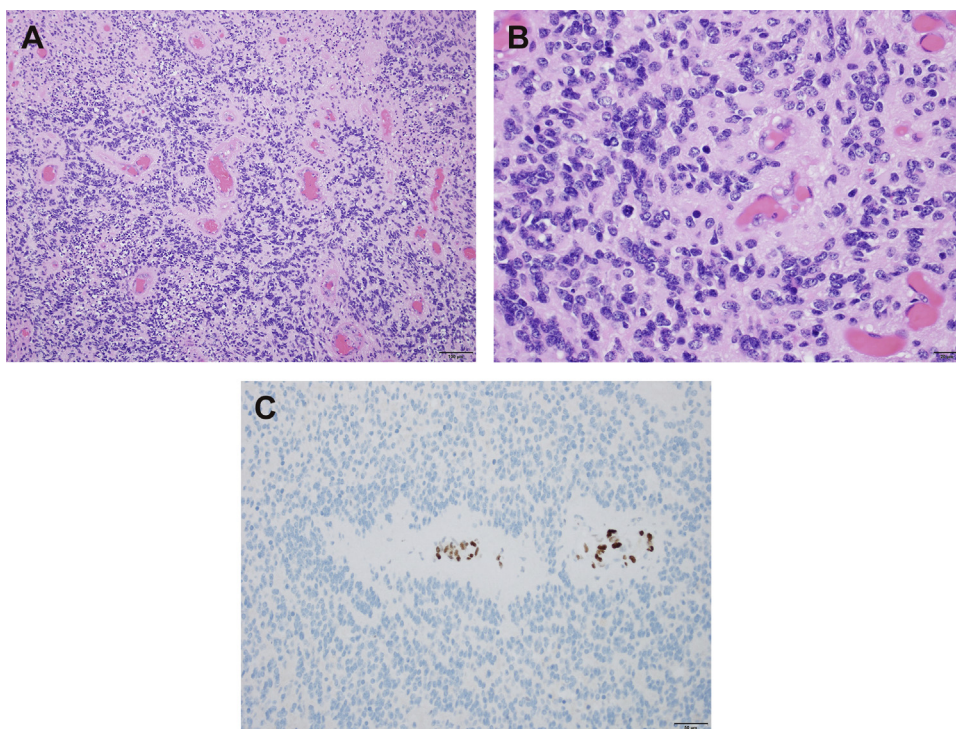
Figure 2 (A) Hematoxylin and eosin−stained sections reveal a hypercellular neoplasm with widespread perivascular pseudo-rosette formation, characteristic of ependymoma (100× magnification). (B) Many regions of the ependymoma are hypercellular and harbor brisk mitotic activity, supporting a diagnosis of anaplastic ependymoma (400× magnification). (C) Ependymoma cells show widespread loss of expression of H3K27me3, and expression is retained in endothelial cells serving as positive internal controls (200× magnification).

dose of 5400 cGy in 30 fractions to the postoperative tumor bed plus a 0.5 to 1.0 cm margin anatomically constrained (clinical target volume [CTV] low) with a cone down of 540 cGy in 3 fractions to the tumor bed, totaling 5940 cGy in 33 fractions (CTV high; Fig 4A). CTV delineation was based on registration of pretreatment diagnostic imaging and postoperative imaging to the CT simulation and MRI in treatment position.

Figure 3 Chromosomal microarray revealed widespread chromosomal instability with loss of whole chromosomes 1, 3, 6, 9, 10, 11, 12, 14, 15, 16, 18, and X in approximately 50% of cells and loss of chromosome 22 in 100% of cells.
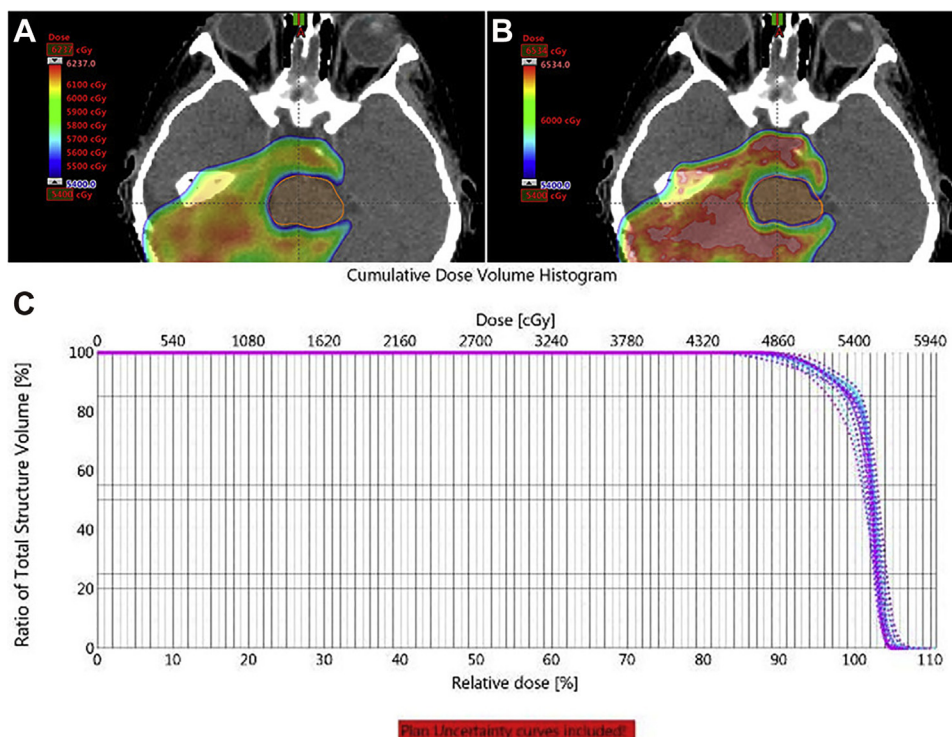
Figure 4   Physical target dose coverage in color wash, (B) biologic model target dose coverage in color wash, and (C) dose-volume histogram robustness curves of target coverage, with solid line representing the target coverage as planned and dashed lines representing robustness for 3 mm of movement and 3% difference in tissue heterogeneity.

A Monte Carlo–based biologic model considering linear energy transfer at the end of the range was used to optimize the biologic dose with respect to organs at risk (OARs; Fig 4B).[14] Robustness curves were generated for 3 mm of movement in the X, Y, or Z direction and for ±3% change in tissue density calculation (Fig 4C). Brainstem constraints were met with planning considerations, including the trade-off between coverage and OARs (Table 2). Daily kV imaging and weekly CT verifications were used.

The patient tolerated treatment, initially under anesthesia, but within the first week he no longer required anesthesia and was able to lie still without discomfort or anxiety. He had moderate skin erythema, patchy alopecia, and continued but improved unsteadiness on his feet, with physical therapy. He had a normal swallow study at the end of treatment, relying on his percutaneous endoscopic gastrostomy tube for hydration but not caloric needs, with anticipated eventual removal. He continues in his first year of follow-up, and his initial imaging after treatment showed no evidence of disease.

Discussion

This patient's case presents multiple considerations in optimal management of pediatric patients with anaplastic ependymoma and the trade-off of the benefits of aggressive intervention with multiple surgeries, CHT, and RT in comparison with treatment morbidity. Additionally, this patient's pathologic findings represent what is thought to be a rare entity: Discordance between chromosomal analysis with multiple abnormalities as defining the PF-EPN-B group, but with H3K27me3 loss of expression, most common in PF-EPN-A (circa ≥99%) and representing a rare finding (approximately 2.5%) in PF-EPN-B.[13]

This case, in the context of prior series investigating extent of surgical resection, PF-EPN grouping, and RT, reveals the challenges inherent in treatment of pediatric patients with PF-EPN and the challenges of future studies attempting to base treatment recommendations on molecular profiling. This patient is best classified in the PF-EPN-B category, but he had a large invasive tumor that required multiple surgeries with the likelihood of, at minimum, significant residual microscopic disease. Furthermore, PF-EPN-B tumors tend to occur in the midline, whereas this lesion was lateralized, making resection more challenging, including extension supratentorially. PF-EPN-B tumors are also much more common in older and typically female patients in comparison with this 8-year-old male patient.[5,6] He had marked chromosomal imbalances, but H3K27me3 expression was lost, which may be an adverse prognostic factor, although there are insufficient data for conclusion.

Table 2   Dose to organs at risk

Organ	Dose
Brainstem	
Maximum point dose	5741 cGy
D0.1 cc	5540 cGy
D50%	4856 cGy
Cochlea (right)	
Maximum	5563 cGy
Mean	4949 cGy
Cochlea (left)	
Maximum	2048 cGy
Mean	1805 cGy
Hippocampus (right)	
Maximum	6039 cGy
Mean	5939 cGy
V23 Gy	100%
Hippocampus (left)	
Maximum	5861 cGy
Mean	2267 cGy
V23 Gy	41.3%
Temporal (right)	
Maximum	6166 cGy
Mean	3007 cGy
Temporal (left)	
Maximum	6111 cGy
Mean	1230 cGy
Pituitary	
V40 Gy	61.2%
Mean	4218 cGy
Spinal cord	
Maximum	4763 cGy

Trials are in development to investigate de-escalation of therapy, including omission of RT for PF-EPN-B patients, but whether treatment de-escalation for this patient would be advisable remains unclear. Recurrences in PF-EPN-B patients can occur late in a patient's course, and surgery alone may be curative in only 50% of patients, making patterns of failure, long-term 10- to 20-year follow-up, and the ability to salvage failures all primary considerations.[15] Within PF-EPN-B patients, heterogeneity exists in terms of molecular features, with potentially 5 distinct subgroups identified by Cavalli et al.[15] Additionally, their analysis revealed loss of 13q as an adverse prognostic factor for progression-free survival (hazard ratio, 3.88; $P = .0041$) whereas 1q gain does not appear to be prognostic for PF-EPN-B (as demonstrated for PF-EPN-A).[15] This extensive work remains to be validated, but further stratification or subgrouping of PF-EPN-B may be possible. The patient presented herein did not have 13q loss or 1q gain.

In summary, multidisciplinary input is warranted, and future trials will need to address the heterogeneity of presentations of an already rare entity: heterogeneities in extent of resection, molecular features, age and related morbidities, and location of disease. Furthermore, the patients who are the most likely to benefit from de-escalation of therapy are those who are least likely to experience the most severe side effects of RT: older patients with midline tumors with potentially less radiation dose to critical OARs. At present, our recommendation is for adjuvant RT as described for all PF-EPN-A and PF-EPN-B patients, with consideration of omission or de-escalation of a carefully selected lowest-risk cohort in the setting of a clinical trial, ideally randomized, with long-term follow up and robust molecular analysis, weighing the impact of adjuvant treatment and primary disease control with deferred RT and the potential for salvage in the setting of recurrence.

Conclusions

Epigenetic profiling of PF-EPN tumors offers an effective way to characterize PF-EPN-A versus PF-EPN-B grouping. However, the optimal management of patients with more favorable PF-EPN-B lesions remains to be determined prospectively, and the best treatment based on current evidence involves gross total resection followed by adjuvant RT. Furthermore, H3K27me3 acts as a sensitive and specific correlate to PF-EPN grouping, but patients such as the case reported herein can have chromosomal abnormalities designating a PF-EPN-B classification but demonstrate H3K27me3 loss of expression. The implications, true frequency, and prognosis of such patients remain to be determined. Further clinical, pathologic, and molecular data are needed to identify select populations in which escalation of therapy is warranted and where de-escalation of therapy may be evaluated in the setting of a clinical trial.

References

1. Hübner JM, Kool M, Pfister SM, Pajtler KW. Epidemiology, molecular classification and WHO grading of ependymoma. *J Neurosurg Sci*. 2018;62:46-50.
2. Merchant TE, Li C, Xiong X, Kun LE, Boop FA, Sanford RA. Conformal radiotherapy after surgery for paediatric ependymoma: A prospective study. *Lancet Oncol*. 2009;10:258-266.
3. Khatua S, Ramaswamy V, Bouffet E. Current therapy and the evolving molecular landscape of paediatric ependymoma. *Eur J Cancer*. 2017;70:34-41.
4. Smith A. ACNS0831: A phase III randomized trial of post-radiation chemotherapy in patients with newly diagnosed ependymoma ages 1-21 years. Available from: https://childrensoncologygroup.org/index.php/acns0831. Accessed July 23, 2018.
5. Pajtler KW, Witt H, Sill M, et al. Molecular classification of ependymal tumors across all CNS compartments, histopathological grades, and age groups. *Cancer Cell*. 2015;2:728-743.
6. Wani K, Armstrong TS, Vera-Bolanos E, et al. A prognostic gene expression signature in infratentorial ependymoma. *Acta Neuropathol*. 2012;123:727-738.
7. Ellison DW, Kocak M, Figarella-Branger D, et al. Histopathological grading of pediatric ependymoma: Reproducibility and clinical relevance in European trial cohorts. *J Negat Results Biomed*. 2011;10:7.

8. Merchant TE, Bendel AE, Sabin N, Burger PC, Wu S, Boyett JM. A phase II trial of conformal radiation therapy for pediatric patients with localized ependymoma, chemotherapy prior to second surgery for incompletely resected ependymoma and observation for completely resected, differentiated, supratentorial ependymoma. *Int J Radiat Oncol Biol Phys*. 2015;93:S1.

9. Tihan T, Zhou T, Holmes E, Burger PC, Ozuysal S, Rushing EJ. The prognostic value of histological grading of posterior fossa ependymomas in children: A Children's Oncology Group study and a review of prognostic factors. *Mod Pathol*. 2008;21:165-177.

10. Pajtler KW, Mack SC, Ramaswamy V, et al. The current consensus on the clinical management of intracranial ependymoma and its distinct molecular variants. *Acta Neuropathol*. 2017;133:5-12.

11. Ramaswamy V, Hielscher T, Mack SC, et al. Therapeutic impact of cytoreductive surgery and irradiation of posterior fossa ependymoma in the molecular era: A retrospective multicohort analysis. *J Clin Oncol*. 2016;34:2468-2477.

12. Bayliss J, Mukherjee P, Lu C, et al. Lowered H3K27me3 and DNA hypomethylation define poorly prognostic pediatric posterior fossa ependymomas. *Sci Transl Med*. 2016;8:366ra161.

13. Panwalkar P, Clark J, Ramaswamy V, et al. Immunohistochemical analysis of H3K27me3 demonstrates global reduction in group-A childhood posterior fossa ependymoma and is a powerful predictor of outcome. *Acta Neuropathol*. 2017;134:705-714.

14. Wan Chan Tseung HS, Ma J, Kreofsky CR, Ma DJ, Beltran C. Clinically applicable Monte Carlo-based biological dose optimization for the treatment of head and neck cancers with spot-scanning proton therapy. *Int J Radiat Oncol Biol Phys*. 2016;95:1535-1543.

15. Cavalli FMG, Hübner JM, Sharma T, et al. Heterogeneity within the PF-EPN-B ependymoma subgroup. *Acta Neuropathol*. 2018;136:227-237.